cause it is simpler to extrapolate than non-linear trends and so is less prone to observer error during an emergency.

The fracturing interpretation, however, was based on a comparison between Eq. 1 and a new relation for Ω derived from the growth of c c c cracks (McGuire and Kilburn, 1997; Kilburn and Voight, 1998). The assumption that large-scale fracturing, which triggers measured seismic events, shows behaviour similar to microscopic cracking was justified retrospectively by the good agreement between expected and observed rates of seismicity. The assumption, however, has not been formally justified.

Eq. 1 has been applied to changes in precursory rates of seismic energy release, ground deformation and seismic event rate (Voight, 1988, 1989; Voight and Cornelius, 1991; Cornelius and Voight, 1995, 1996; McGuire and Kilburn, 1997; Kilburn and Voight, 1998; De la Cruz-Reyna and Reyes-Dávila, 2001; Reyes-Dávila and De la Cruz-Reyna, 2002). Of these, seismic event rate is the most useful during an emergency because it is simple to measure, even with a temporary monitoring network, and requires minimal data processing. Accordingly, this paper will focus on how seismic event rate can be related to the macroscopic development of crack populations and the propagation of a pathway that allows magma to breach the surface. By concentrating on the extension of a fracture system, the analysis is implicitly directed towards changes in the rate of volcano-tectonic (VT) events, rather than the long-period (LP) events that are commonly associated with pressure changes induced by fluids (e.g. magma, released magmatic volatiles or meteoric fluids) migrating through fractures (Chouet, 1996; McNutt, 2000).

3. Features of pre-eruptive seismicity

Short-term pre-eruptive seismicity normally evolves at depths of less than 5–7 km (McNutt, 1996). Events tend to cluster (a) beaneath the volcano's axis, within an approximately cylindrical region some 1–3 km across (Fig. 3) and, especially during the initial stages of unrest, also (b) around one or more locations with epicentres offset from the axis by several kilometres (Aspinall et al., 1998; De Natale et al., 1991; McNutt, 1996; Harlow et al., 1996). Although events of magnitude 5–6 have been recorded (Smith and Ryall, 1982; Savage and Cockerham, 1984), most have magnitudes less than 2 (Hill et al., 1990; McNutt, 1996). For magnitudes of 0–2, the events are associated with movements of about 1–10 mm over corresponding distances of 10–100 m (McNutt, 2000).

During the final acceleration to eruption, which evolves over intervals of $\sim$1–10 days and is often dominated by events within the 'seismic cylinder' beneath the volcano's axis, the total number of events with magnitudes of about 1 or more is frequently $\sim 10^2$–10^3 (Figs. 6 and 7). The implied cumulative displacement is thus $\sim$10 m or less. In comparison, magma bodies triggering the precursors have notional lengths of $\sim$1 km and must force their way at least through $\sim$1 km of a volcanic edifice. Apparently, the detected events cannot be explained by the simple upward displacement of a dyke. Indeed, events often occur throughout the whole axial seismic cylinder during the entire precursory sequence without a strongly preferred upward migration (Aspinall et al., 1998; Harlow et al., 1996). The simplest interpretation is that cracks grow throughout the whole axial seismic cylinder before they eventually join together an array of previously isolated fractures. Once connected, these fractures form the new pathway for magma ascent. Because the key objective of this paper is to investigate the use of accelerating seismicity for forecasting eruptions, the analysis concentrates on events triggered within the axial seismic cylinder (Fig. 3). The role of non-axial seismic clusters is left for evaluation elsewhere.

Precursory events are commonly dominated by reverse and strike-slip faulting. Such behaviour is consistent with slip movements under compressional stress (due to gravitational loading and to magmatic overpressure) in rock surrounding an array of subvertical fractures (Fig. 3). Thus, even in a compressional field, subvertical fractures can be preferentially reactivated when compression is smaller horizontally than vertically, while

therefore focusses on how energy is supplied for creating new crack surfaces and for controlling observed rates of seismicity.

5. Seismic event rates and stress £uctuations

Detected seismic events are produced as faults grow between the ends of widening, subvertical fractures (Fig. 3). Fault extension itself is controlled by processes operating within the zone of stress concentration, or *c* , that develops around the fault's tip when it is put under stress (Atkinson, 1984; Main, 1991; Main and Meredith, 1991; Lockner, 1993; Cowie and Shipton, 1998). Within this zone, arrays of smaller, tensile cracks and slip surfaces grow and coalesce until the whole zone is broken, so extending the parent fault (Fig. 4). However, just as a large fault grows by the extension and coalescence of small cracks around its tips, so each of the small cracks also grows by the extension and coalescence of the next smaller population of cracks in its own process zone. Fracturing is thus viewed as a multiscale process, major fractures being the result of cracking at successively smaller scales, down to the submicroscopic dimensions at which cracks nucleate. Excluding nucleation events, therefore, it should be possible to resolve a recorded event into a sequence of growth steps among smaller cracks whatever the scale of observation (Fig. 4).

As a crack of any size extends, it releases energy by relaxing the strain in the rock immediately around its new extension, but consumes energy in creating and separating the new crack surfaces (e.g. Lawn, 1993). Extension continues as long as the energy released exceeds the amount consumed. Among a population of cracks, however, the overall pattern of growth is complicated by interference between neighbouring cracks. Thus, the zone of stress concentration around a crack tip is

geometry of the monitoring array, the depth of fracturing, and the attenuating properties of the fracturing medium) cannot be distinguished individually but, instead, they control the frequency of the background variation in stress. The number of events detected seismically then depends on the rate at which the background stress is locally high enough to extend fractures that are larger than the threshold value.

5.1. Q a a c ac

Assuming that stress fluctuations occur randomly in a volume under stress, the probability of crack propagation is given by the proportion of cracks that have the required additional strain energy around their tips at any particular moment. If the volume consists of ϕ a controlling cracks (where ϕ is large), then the number of ways Θ that random energy fluctuations will yield ac cracks, with the strain energy ε necessary for propagation, is:

$$\Theta = \emptyset!/\prod\ !\qquad (4)$$

Importantly, it is not necessary to specify which particular members of the crack population are active at any given moment, but only the number that are active. The problem thus becomes analogous to the classical Boltzmann analysis in statistical physics of describing the energy distribution among a large population of randomly moving gas molecules (and, hence, of deriving the associated gas pressure) for which it is important to know the total number of molecules in a particular energy state, rather than to follow the changes in energy state of individual molecules (Ruhla, 1992). Following the Boltzmann analysis (Ruhla, 1992; Landau and Lifshitz, 1999), therefore, the probability $\mathrm{P}(\varepsilon)$ that a crack tip is supplied with the extra energy ε is given by determining the maximum value of Θ, which corresponds to the state of statistical equilibrium:

$$\mathrm{P}(\varepsilon) = \frac{[\text{Number of ways of containing energy } \varepsilon]}{[\text{Total number of energy states available}]}$$

$$= (1/Z)\mathrm{e}^{-\varepsilon/RT} \qquad (5)$$

where the total internal energy RT consists of the ideal gas constant, R (8.314 J mol^{-1} K^{-1}), absolute temperature, T, and the number of moles of rock involved in cracking a process zone; although originally determined from gas thermodynamics, the use of R is valid also for the internal energy of solids. The partition function $Z = \Sigma\, \mathrm{e}^{-\varepsilon/RT}$ measures the total number of energy states in which a crack tip could exist.

The probability of cracking in Eq. 5 can be transformed into expected rates of cracking, by introducing the mean frequency of stress fluctuations, so that $\mathrm{d}N(\ )/\mathrm{d}$, the expected crack rate (or rate of successful stress fluctuations for crack extension), becomes $\mathrm{P}(\varepsilon)$. Given that and Z are constant for a given system, it follows that:

$$\mathrm{d}N(\ )/\mathrm{d} = {}^{*}\mathrm{e}^{-\varepsilon/RT} \qquad (6)$$

where $^{*} = /Z$.

Eq. 6 combines cracking at different scales through the exponent and pre-exponential term on its right-hand side. Thus, while * describes the rate of stress fluctuations (involving those due to cracking at sizes too small to be resolved), the term $\mathrm{e}^{-\varepsilon/RT}$ describes the proportion of those fluctuations that provide the energy ε for activating the cracks that can be detected. Importantly, no constraints have been imposed on *ab* crack size, so that the form of Eq. 6 should be valid for rates of cracking at all scales (although some limits will be introduced later).

Eq. 6 provides a second link between fracturing at different scales, by noting that each event N corresponds both (a) to a growth step for one member of a population of fractures of a particular size (at, say, Scale 1), and (b) to a cycle of growth and coalescence among the smaller cracks (Scale 2) in the process zone of the Scale-1 fracture (Fig. 4). Coalescence terminates the acceleration in Scale-2 event rate and so coincides with the peak rate achieved by the Scale-2 cracks (Fig. 5). Accordingly, a Scale-1 growth step can be expressed in terms of the peak rate of Scale-2 cracking by:

$$\mathrm{d}N_1/\mathrm{d} = \Psi \mathrm{d}N_{2\mathrm{P}}/\mathrm{d} \qquad (7)$$

where, to simplify notation, $N(\ )$ is replaced by N and understood to be a function of time, the subscripts 1 and 2 denote the scale of cracking, sub-

script P denotes peak value, and Ψ is the scaling factor ($\Psi < 1$). This relation will be used later to relate detected seismicity to fracturing at different scales.

By utilising the Boltzmann distribution in Eq. 5, the derivation of Eq. 6 assumes an equilibrium size–frequency distribution for the values of background energy ε, smaller values having a greater frequency of occurrence. For the event rate to accelerate, therefore, the preferred value of ε for further cracking must decrease with time (such that the associated frequency of occurrence increases). The next section describes how such a condition occurs naturally as propagating fractures release the strain energy already stored in the host rock.

5.2. E a a d a c ac

Persistent slow cracking is maintained while the rate of energy released by crack growth just exceeds that required for new cracks to form. From standard theory, this quasi-equilibrium condition can be related to the total change in energy ε in Eq. 6 by (e.g. Griffith, 1920; Jaeger, 1969; Scholz, 1990; Lawn, 1993):

$$\varepsilon = \varepsilon_{NS} - \varepsilon_{G} \tag{8}$$

where ε_{NS} is the energy required to create new fracture surfaces, and ε_{G} is the excess strain en-

recalling that N

bility P(ε) with P(E), analogy with the development of Eq. 6 yields for the frequency of crack events:

$$\mathrm{d}N/\mathrm{d} \quad = (\nu/Z)\mathrm{e}^{-E/\ RT} \tag{16}$$

where is now the number of moles involved in the chemical reactions that cause a crack to extend, and Z is the appropriate partition coefficient.

As with ε in Eq. 6, E de[illegible]H5orH5or

events sucHHP©)crfitTqEBG9I©7H7%fEPfi©mol©V%@f)JT%jEPzBH7%fSPGSzHfi©

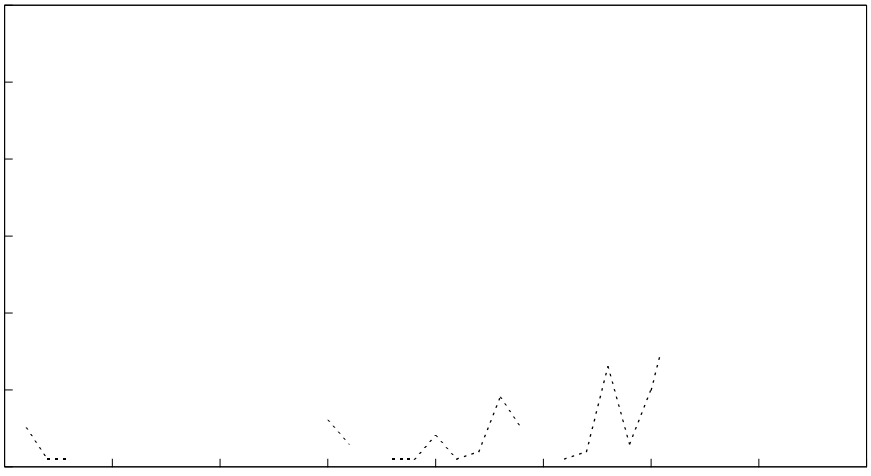

later than observed. By 12 November, the estimate would have been revised to 15 November. Potentially, therefore, a reliable forecast could have been made 3–6 days ahead of the eruption.

6.2. M P a b , L , P , 1991

Seismic monitoring provided the primary data for evaluating the possibility of renewed activity at Mt Pinatubo in 1991, following a repose interval of some 500 years (Cornelius and Voight, 1996; Harlow et al., 1996). After magma broke the surface as a lava dome on 07 June, activity evolved to a climactic plinian eruption on 15 June. The present analysis focusses only on seismicity before the appearance of the lava dome.

Seismicity during the week before dome emplacement was characterised by an acceleration in event rate from about 10 to 60 events every 4 h (Fig. 7; Harlow et al., 1996). Between 01 and 04 June, most of the recorded earthquakes had magnitudes greater than or equal to 0.4 and were located at depths of 1–5 km about 4–5 km northwest of the volcano's summit; after 04 June, in contrast, seismicity was dominated by events with magnitudes of 1.2 or greater and located at less than about 3 km below the future summit vent (Harlow et al., 1996). The seismicity shown in Fig. 7 refers only to events recorded within the axial seismic cylinder (Harlow et al., 1996).

Harlow et al. (1996) postulated that the accelerating rate of seismicity was produced by intense brittle fracturing as magma pushed its way to the surface. Indeed, from 03 to 04 June, the 4-hourly event rate for sub-summit earthquakes shows a clear oscillation about an increasing mean trend (Fig. 7). When plotted on an inverse-rate diagram (Fig. 7), the sequence of minimum values follows a negative linear trend with time, described by:

$$(\mathrm{d}N_{\mathrm{P}}/\mathrm{d}\ )^{-1} =$$

eruption. Moreover, the inverse peak values (minima on the inverse-rate plot) may be easier to identify by eye than the actual peak values (on the event-rate plot) under emergency conditions (compare, for example, Fig. 6a,b).

Applied to the observed precursors (Figs. 6 and 7), the measured values of γ^* are within the range of $(4.5 \pm 3.2) \times 10^{-3}$ expected for conditions within a subvolcanic system. Such agreement is excellent and not only supports the validity of the slow-fracture model, but also suggests that reliable forecasts of eruption might eventually be feasible at least 2–3 days ahead of time. Warning intervals of days are relevant in practice because they may permit successful evacuation of threatened districts.

The restricted range for γ^* is another feature with possible forecasting implications. It is a natural consequence of using peak rates of process-zone cracking as a proI7qHPSby measure for growth steps among the parent fractures, since this substitution cancels terms that depend on crack-tip geometry. Seismic monitoring systems, however, are deployed to detect as many events as possible. It is thus by happy circumstance, rather than by design, that the majority of detected events ap-

earthquake or an intense seismic swarm. Thus, although eruptions may be preceded by seismic sequences similar to those analysed here, it is not evident that all such sequences inevitably lead to eruption. They may instead be followed by a permanent decay in activity or by a temporary lull in seismicity (McNutt, 1996). To guarantee an eruption, therefore, additional criteria must also be satisfied. Such criteria may be deterministic (e.g. the volcanic edifice may first have to be stretched by a critical amount) or stochastic (e.g. whether or not a fracture intersects a magma body may contain an element of chance, perhaps due to edifice heterogeneity). In either case, the present analysis provides a basis on which new studies can build for identifying the additional pre-eruption requirements.

The present model also assumes that, in the final approach to eruption, detected seismicity is dominated by events driven by magmatic pressure applied axially below the future eruptive vent. It does not account (a) for seismicity induced by factors other than magma pressure, such as thermal cracking, or (b) for detected events due to fracturing at locations away from the axial seismic cylinder. Future analyses may be able to filter out signals produced by non-magmatic stresses, while the eventual real-time location of events would distinguish fracturing within and outside the axial seismic cylinder.

The slow-fracture model is a natural extension of the pioneering studies by Voight (1988, 1989) and their development by Voight and Cornelius (1991) and Cornelius and Voight (1994, 1995, 1996). Unlike the present model, which focusses on changes in peak seismic event rate, the previous studies concentrated on changes in mean event rate. The Voight and Cornelius studies also suggested that, in addition to linear decreases with time, inverse rates may on occasion decay exponentially with time (corresponding to the condition $\alpha = 1$ in Eq. 1). Such decay would approach a zero inverse rate (time of eruption) after an unspecified interval and so cannot be used for eruption forecasting, unless independent arguments can also identify a non-zero threshold rate of seismicity at which an eruption is expected. This behaviour has been attributed to the growth of cracks that do not eventually coalesce and so do not lead to the opening of a new magmatic pathway (McGuire and Kilburn, 1997; Kilburn and Voight, 1998); as discussed above, contributors to such cracking may include non-magmatic stresses and events occurring outside the axial seismic cylinder. However, such behaviour might also represent a condition for which a rate-dependent resistance, perhaps along moving faults (Dieterich, 1992), becomes large enough to inhibit further slow fracture. Thus, a more complete form of Eq. 22a may be:

$$\mathrm{d}N_{\mathrm{P}}/\mathrm{d} \quad = \beta \mathrm{e}^{\gamma^* N_{\mathrm{P}}} - \quad (R) \tag{23}$$

where the resisting term (R) is small for conditions that finally result in eruption. The significance of such a resisting term awaits future study.

8. Conclusions

The present model argues that the final stages of magma ascent are controlled by the slow fracturing of host rock between a magma body and the surface. Fracturing occurs by the growth and coalescence of pre-existing cracks. Each crack itself has a process zone containing even smaller cracks. Failure is thus perceived as a multiscale process for which microscopic cracking can ultimately lead to macroscopic fracturing. Since similar processes are assumed to operate at all scales, the form of the governing crack-growth equation

Acknowledgements

This paper benefitted from discussions with Peter Sammonds and Valentina Rocchi (both at UCL) and from helpful reviews by Sebastien Chastin (University of Edinburgh) and Steve McNutt (Alaska Volcano Observatory). The research was funded by the European Commission (DG Research, Environment and Climate programme, Natural Risks, A. Ghazi, Head of Unit, Maria Yeroyanni, Scientific Officer) for Project Volcalert (CEC Contract No. EVG-2001-00040) and by the Gruppo Nazionale per la Vulcanologia, Italy.

Appendix. Manipulation of the event-rate equation

From Eq. 12 in the main text:

$$\mathrm{d}N/\mathrm{d} = C\mathrm{e}^{\gamma N} \quad \text{(A1)}$$

where the constant $C = {}^{*}\mathrm{e}^{-\eta}\mathrm{e}^{\gamma c_0/\Delta c}$.

Rearrangement of Eq. A1 leads to:

$$\int_{N_0}^{N} \exp(-\gamma N)\mathrm{d}N = C\int_{0} \mathrm{d} \quad \text{(A2)}$$

which yields:

$$(\mathrm{e}^{-\gamma N_0}/C) - (\mathrm{e}^{-\gamma N}/C) = \gamma(-{}_0) \quad \text{(A3)}$$

Noting from Eq. A1 that $(\mathrm{d}N/\mathrm{d})^{-1} = \mathrm{e}^{-\gamma N}/C$, Eq. A3 becomes:

$$(\mathrm{d}N/\mathrm{d})^{-1} = (\mathrm{d}N/\mathrm{d})_0^{-1} - \gamma(-{}_0) \quad \text{(A4)}$$

where $(\mathrm{d}N/\mathrm{d})_0$ is the value of $\mathrm{d}N/\mathrm{d}$ at $= {}_0$, identical with Eq. 13 in the main text.

The values of ${}_0$ and, hence, of $(\mathrm{d}N/\mathrm{d})_0$ are normally determined empirically from graphs of accelerating event rate. However, $(\mathrm{d}N/\mathrm{d})_0$ can in principle also be calculated from Eq. A1 as ${}^{*}\mathrm{e}^{-\eta}\mathrm{e}^{\gamma c_i/\Delta c}\mathrm{e}^{\gamma N_0}$ or, using Eq. 11, as ${}^{*}\mathrm{e}^{-\varepsilon_0/RT}$ where ε_0 is the excess energy required to start the acceleration in rate of rock fracturing.

References

Anderson, O.L., Grew, P.C., 1977. Stress corrosion theory of crack propagation with applications to geophysics. Rev. Geophys. Space Sci. 15, 77–104.

Aspinall, W.P., Miller, A.D., Lynch, L.L., Latchman, J.L., Stewart, R.C., White, R.A., Power, J.A., 1998. Soufrière Hills eruption, Montserrat, 1995-1997: Volcanic earthquake locations and fault plane solutions. J. Geophys. Res. 25, 3397–3400.

Atkinson, B.K., 1984. Subcritical crack Sci. 15,MontsVolcP5BE)89nallTl

pines. PHIVOLCS, Quezon City, and University of Washington Press, Seattle, WA, pp. 285–305.
Heimpel, M., Olson, P., 1994. Buoyancy-driven fracture and magma transport through the lithosphere: models and experiments. In: Ryan, M.P. (Ed.), Magmatic Systems. Academic Press, San Diego, CA, pp. 223–240.
Hill, D.P., Ellsworth, W.L., Johnston, M.J.S., Langbein, J.O., Oppenheimer, D.H., Pitt, A.M., Reasenburg, P.A., Sorey, M.L., McNutt, S.R., 1990. The 1989 earthquake swarm beneath Mammoth Mountain, California: an initial look at the 4 May through 30 September activity. Bull. Seism. Soc. Am. 80, 325–339.
Jaeger, J.C., 1969. Elasticity, Fracture and Flow, 3rd edn. Chapman and Hall, London, 268 pp.
Kilburn, C.R.J., Voight, B., 1998. Slow rock fracture as eruption precursor at Soufriere Hills volcano, Montserrat. Geophys. Res. Lett. 25, 3665–3668.
Landau, L.D., Lifshitz, E.M., 1999. Statistical Physics, Part 1, 3rd edn. Butterfield Heinemann, 546 pp.
Lawn, B., 1993. Fracture of Brittle Solids, 2nd edn. Cambridge University Press, Cambridge, 378 pp.
Lister, J.R., 1991. Steady solutions for feeder dykes in a density-stratified lithosphere. Earth Planet. Sci. Lett. 107, 233–242.
Lockner, D., 1993. Room temperature creep in saturated granite. J. Geophys. Res. 98, 475–487.
Main, I.G., 1991. A modified Griffith criterion for the evolution of damage with a fractal distribution of crack lengths: application to seismic event rates and *b*-values. Geophys. J. Int. 107, 353–362.
Main, I.G., Meredith, P.G., 1991. Stress corrosion constitutive laws as a possible mechanism of intermediate-term and short-term seismic event rates and *b*-values. Geophys. J. Int. 107, 363–372.
Main, I.G., 1999. Applicability of time-to-failure analysis to accelerated strain before earthquakes and volcanic eruptions. Geophys. J. Int. 139, F1–F6.
Main, I.G., 2000. A damage mechanics model for power-law creep and earthquake aftershock and foreshock sequences. Geophys. J. Int. 142, 151–161.
Marder, M. Fineberg, J., 1996. How things break. Physics Today (September) 24–29.
McGuire, W.J., Kilburn, C.R.J., 1997. Forecasting volcanic events: some contemporary issues. Geol. Rundsch. 86, 439–445.
McGuire, W.J., Kilburn, C.R.J., Murray, J.B. (Eds.), 1995. Monitoring Active Volcanoes: Strategies, Procedures and Techniques. UCL Press, London, 421 pp.
McNutt, S.R., 1996. Seismic monitoring and eruption forecasting of volcanoes: a review of the state-of-the-art and case histories. In: Scarpa, R., Tilling, R.I. (Eds.), Monitoring and Mitigation of Volcano Hazards. Springer, Berlin, pp. 99–146.
McNutt, S.R., 2000. Volcano seismicity. In: Sigurdsson, H. (Ed.), Encyclopedia of Volcanoes. Academic Press, San Diego, CA, pp. 1015–1033.
Newhall, C.G., Punongbayan, R.S. (Eds.), 1996. Fire and Mud: Eruptions and Lahars of Mount Pinatubo, Philippines. PHIVOLCS, Quezon City, and University of Washington Press, Seattle, WA.
Power, J.A., Wyss, M., Latchman, J.L., 1998. Spatial variations BatiH7qHP5Ez57%@f[VBlzeism0EPnonHM.
tions19Efi,SeEsm0EPnstafiJ.,